



**HAL**  
open science

## Experimental and analytical study of hybrid steel-timber beams in bending

Bruno Jurkiewicz, Sebastien Durif, Abdelhamid Bouchaïr, Cécile Grazide

► **To cite this version:**

Bruno Jurkiewicz, Sebastien Durif, Abdelhamid Bouchaïr, Cécile Grazide. Experimental and analytical study of hybrid steel-timber beams in bending. *Structures*, 2022, 39, pp.1231-1248. 10.1016/j.istruc.2022.03.055 . hal-04116108

**HAL Id: hal-04116108**

**<https://hal.science/hal-04116108>**

Submitted on 6 Jun 2023

**HAL** is a multi-disciplinary open access archive for the deposit and dissemination of scientific research documents, whether they are published or not. The documents may come from teaching and research institutions in France or abroad, or from public or private research centers.

L'archive ouverte pluridisciplinaire **HAL**, est destinée au dépôt et à la diffusion de documents scientifiques de niveau recherche, publiés ou non, émanant des établissements d'enseignement et de recherche français ou étrangers, des laboratoires publics ou privés.

# ***Experimental and analytical study of hybrid steel-timber beams in bending***

**JURKIEWIEZ Bruno<sup>1\*</sup>, DURIF Sébastien<sup>2</sup>, BOUCHAIR Abdelhamid<sup>2</sup>, GRAZIDE Cécile<sup>1</sup>**

<sup>1</sup> *Université de Lyon, Université Claude Bernard Lyon 1, Laboratory of Composite Materials for Construction (LMC<sup>2</sup>), 82 boulevard Niels Bohr, 69100 Villeurbanne, France.*

<sup>2</sup> *Université Clermont Auvergne, Clermont Auvergne INP, CNRS, Institut Pascal, F-63000 Clermont-Ferrand, France*

*\*Corresponding author. Tel.: +33 04 72 69 20 71- Fax: +334 72 69 21 20 (B. Jurkiewicz)*

*E-mail addresses: [bruno.jurkiewicz@univ-lyon1.fr](mailto:bruno.jurkiewicz@univ-lyon1.fr) (B. Jurkiewicz), [sebastien.durif@uca.fr](mailto:sebastien.durif@uca.fr) (S. Durif), [abdelhamid.bouchair@uca.fr](mailto:abdelhamid.bouchair@uca.fr) (A. Bouchair), [cecile.grazide@univ-lyon1.fr](mailto:cecile.grazide@univ-lyon1.fr) (C. Grazide).*

## **ABSTRACT:**

The combination of timber elements and steel beams can be of high interest for mechanical performances including instabilities and fire protection. In this paper, experiments and numerical modelling are performed to analyse the behavior of various configurations of steel-timber beams in bending. Two timber beams are connected to the web and the flanges of the steel beam. In order to define the material properties of the tested elements, each component (wood and steel) has been tested separately. Then, timber and steel beams have been connected and tested up to failure. The observed behavior shows a limited effect of hybridization in the elastic domain. However, the effect is significant at the ultimate stage. Actually, the combination of timber and steel elements improves the resistance to lateral torsional buckling and local buckling of the steel beam. The stiffness and the strength of these innovative hybrid structures are estimated at SLS and ULS respectively using approaches similar to those proposed in European design rules. The analytical values are close to those obtained from tests even with the failure reached by instability of steel element. However, it appears that for hybrid beams the calculated value of elastic critical bending moment for lateral-torsional buckling needs to be improved. These results highlight the potential of the steel-timber hybrid elements for further developments.

**KEYWORDS:** Steel-timber element, Structural wood, Hybrid structures, Experiments, Design analysis.

## **1 Introduction**

Steel structures are easy to connect and steel material performs high strength characteristics leading to relatively slender elements. Furthermore, the use of steel can highly increase the stiffness and the ductility of structures. Moreover, timber structures provide a welcoming touch in comparison to other structural materials. Generally, steel is used to reinforce timber structures as both materials are characterized by a high strength to weight ratio. Thus, high flexural stiffness can be obtained with controlled dimensions of cross-sections mainly to optimize the floor thickness [1]. Structures combining steel and wood elements show pleasant visual aspect and high mechanical performances regarding stiffness, strength and ductility. These high performances are particularly appreciated under seismic actions [2]. Another interest of coupling both materials can be for fire resistance. Indeed, the Building Research Institute in Japan performed 4-hours fire resistance tests on steel profiles encased in different glued-laminated timber elements. Other similar studies have been led by Kashihara et al. [3] in Japan on a five-storey building.

However, the combination of both materials remains a difficult challenge for designers due to the differences in physical and mechanical characteristics. Indeed, steel and wood are very different materials with specific mechanical, thermal and physical performances. Steel is a manufactured product, predictable and infinitely recyclable. Wood is a natural and renewable material, with significant variability in strength and stiffness. Both materials behave in different ways under environment conditions: steel is affected by temperature variations whereas wood is influenced by

changes in humidity. These parameters need to be well controlled in the design process of hybrid solutions combining the two materials.

Steel-timber hybrid structures have been investigated in several studies at the end of the 20th century in order to obtain efficient hybrid floors. Steel beams can be connected to CLT panels through mechanical connectors or adhesives. These hybrid structures showed very interesting mechanical properties regarding the stiffness, the resistance and the ductility [4-7].

Generally, the main researches carried out concern the strengthening of timber elements and steel is one of the materials that can be used as mechanical reinforcement. Bulleit et al. [8-9] and Borri et al. [10] analysed the behavior of timber beams reinforced with embedded steel bars in order to improve the performances in bending. Although this solution is difficult to implement because of the wood sensitivity to hydric transfers, it was used with applications mainly in the rehabilitation of existing structures [1]. Figure 1 presents an example of reinforcement of old existing timber beams where steel bars were inserted and bonded using epoxy resin. This process is known as ‘modified flitch beams’. Alam et al. [11] studied different types of bonded-in reinforcements including steel to repair damaged wood beam (Figure 2). Their results showed the high performance of reinforcements on the upper and lower faces, as steel was optimized at the location of maximal bending stresses. However, the authors pointed out the cost of this type of solution and especially the aesthetical impact related to apparent steel reinforcements.

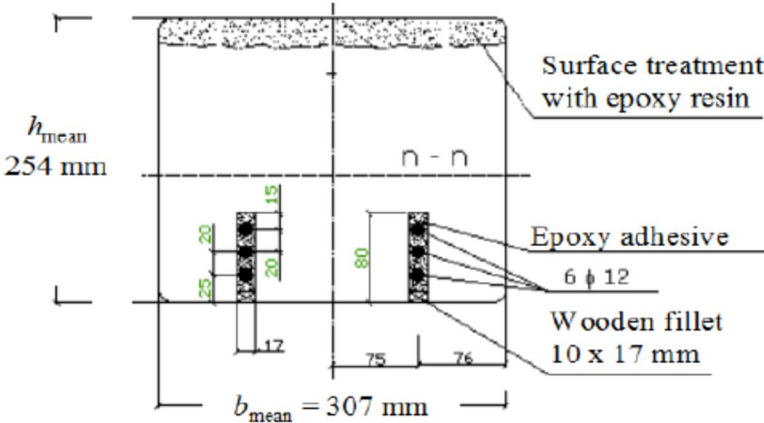


Figure 1: beam upgrade using steel bars and epoxy pouring resin in modified flitch beams [1]

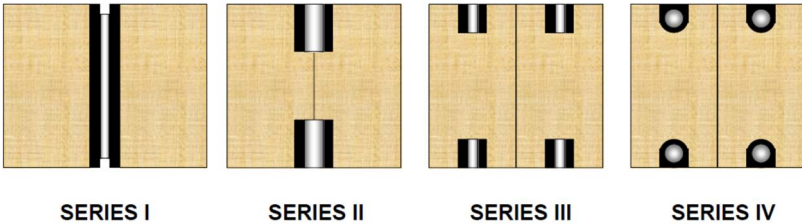


Figure 2: timber beams reinforced by steel plates or bars [11, 18]

Another way to use steel to strengthen timber beams is based on high strength steel cord or Steel Fiber Reinforced Polymers (SFRP) bonded to wood elements. Borri and Corradi [12] made tests on wood beams reinforced with high strength steel fibers and showed a significant increase in ultimate strength and ductility. However it has been observed a relatively small influence in the elastic stiffness as it could be observed for composite reinforcements such as FRP [13, 14]. Indeed, similar process can be found using FRP reinforcements, but those systems are not in the scope of the present study. Ghanbari-Ghazijahani et al. [15] studied composite equal leg angles to strengthen beams and observed

that those steel angle sections made the beams considerably stronger in bending and increased the stiffness.

The usual concept of timber beams reinforced by steel sections concerns the flitch plate beams. Those beams are composed of two timber elements with a single or double intermediate steel plates (Figure 3). The wood sidepieces provide lateral support to the steel plate against lateral buckling. Both wood and steel share the load proportionally to their relative stiffness. Jasienko and Nowak made several experimental tests on timber beams strengthened with steel plates [16]. Those tests concerned both new and old woods. Their results were compared to FRP strengthening techniques and the authors found comparable performances. Those plates were directly bonded to the wood elements even if the authors indicate that for safety reasons, some nails should be added to secure the connection in case of fire. The same authors give a detailed review and experimental tests on timber beams reinforced with steel plates [17]. The main observations are that the use of bonded steel plates allows to increase both strength and stiffness in a similar or better way than FRP solutions. However, before using epoxy, the combination of steel and timber was generally based on mechanical connections. Various types of steel plates have been used, either for shear strengthening or bending strengthening. It was also reported in [17] that Hairstans et al. studied an innovative solution to connect the steel plates with timber elements in order to propose a less time-consuming solution using shot fired dowels as it limits the number of arduous tasks as pre-drilling and bolting.

Alam et al. [18] pursued the study on steel plate flitch beams. They pointed out the need to ascertain the effect of nail density on the beam strength and stiffness. The research concerned specifically the shot-fired nailing technique. Those studies allowed to conclude that the flexural modulus did not increase as a function of increasing nailing density. This shows that the contribution of steel to the stiffness of the hybrid composite beam is achieved with the lowest nailing density. Furthermore, it has been observed that increasing too much the nailing density may reduce the global strength as it can make crack propagation easier in the wood. However, low nail density around the most compressed parts induces a strength decrease by buckling of the steel plate.

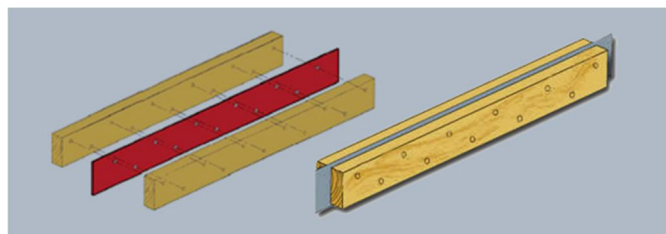


**Figure 3: illustration of a flitch plate beam**

Finally, Corradi et al. [19] proposed an exhaustive review on the solutions to repair timber structures using either stainless steel L-shape sections or a tee section (flitch plate with a bottom flange). This review presents also the solutions with stainless steel plates bonded or screwed on the bottom of timber beams. Indeed, using steel or stainless steel in the most tensile areas ensure the best bending strengthening as for fibers or steel reinforced polymers strengthening. The authors emphasize the interest of using mechanical connection devices instead of bonded connections. Indeed, mechanical connection makes the structure removable which can be an important issue in order to provide some reversibility of the reinforcement or for a better recyclability of both materials.

As seen hereafter, the main of the research works performed on hybrid steel-timber structures focused on the reinforcement of timber structures by steel. The present study takes a different point of view considering hybrid beams composed of steel and wood elements where wood is used to reinforce the steel profile [20-22]. Recent research works on steel-timber columns showed the interaction between timber and steel elements. The experimental tests led on hybrid columns, made of H shaped steel sections embedded in glued laminated timber, failed by global buckling [23]. The authors observed that glulam reinforced the steel column improving thus its buckling strength.

It has been seen in the case of steel flitch beams that timber plays the role of lateral support against buckling of the plate. However, using a plate does not allow efficient use of steel leading to heavier profiles without efficient improvement of the bending properties [24]. The main aim of the present study is to evaluate the mechanical reinforcement provided by wood elements to steel profiles, especially against instability such as lateral torsional buckling or local buckling.

Thus, this study focuses on the experimental evaluation of the mechanical behavior of hybrid steel-timber profiles in bending. Furthermore, the timber beams used in the tests contained numerous knots. Indeed, the objective of those tests consists in evaluating the potential use of ungraded wood provided by a local supplier of the region AURA (Auvergne Rhône Alpes) in France. This study aims to evaluate the capacity of timber elements to provide efficient lateral support against local buckling and to improve the elastic and plastic bending strengths.

The first part of this paper is dedicated to the characterization of the material properties. The timber elements used in the tests have several defects. Thus, it has been decided to conduct several bending tests to evaluate the influence of knots on their stiffness and strength. The second part of the paper focuses on bending tests performed on steel-timber hybrid beams up to failure. The global behavior, the performances and the failure modes are presented, analysed and discussed. Finally, simplified analytical models are used to compare calculated results to measurements of the elastic stiffness and the failure load. Discrepancies are addressed and discussed.

## 2 Experimental program

Tests concerned basic materials (steel and timber) and full-scale steel, timber and hybrid beams (3 meters span). Wood is a natural material usually considered as orthotropic and may present defects (such as knots, variation of density, slope of wood grain...). Figure 4 presents an example of wood element used in the hybrid beams. It can be seen that the timber elements exhibited numerous defects which could imply their reject according to the visual grading of NF B 52-001-2 [25]. Thus, in addition to full-scale wood beams, smaller specimens are cut for material tests.



**Figure 4: example of timber elements used in hybrid beam tests in the study**

### 2.1 Materials properties

Materials properties were determined by means of tensile tests for steel and bending tests for wood on different geometries.

Three specimens have been cut from the IPE 160 profile used for the full-scale bending tests. They were tested in tension according to ISO 6892-1:2019 standard.

The wood moisture content was determined by oven dry method, following the European standard EN 13183-1 [26]. The oven temperature has been fixed at 105°C and the samples remained in the oven during 2 days to reach a constant weight.

In order to obtain the elastic modulus and the strength of wood, bending tests have been carried out on 21 specimens according to the European standard rules EN 408 [27]. Thus, several dimensions have been tested to evaluate the influence of knots on the mechanical properties of the wood in bending. Specimens with different lengths ranging from 346 to 900 mm were tested. The standard EN 408 defines two different elastic modulus: the local ( $E_{m,l}$ ) and global ( $E_{m,g}$ ) modulus of elasticity. Both were evaluated by means of a 4-point bending test. The global modulus of elasticity was obtained through the measurement of the vertical displacement at the mid-span of the specimen. The local modulus was obtained considering the relative displacement between the mid-span and two symmetrically positioned points with a spacing equal to  $5h$  ( $h$ : specimen height). Figure 5 presents the test set-up and the position of the different measuring tools.

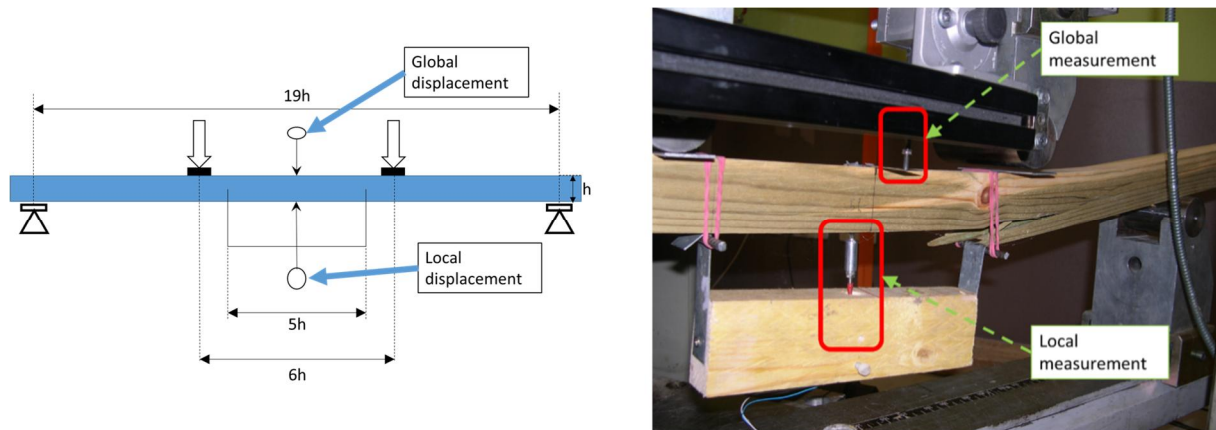


**Figure 5: 4-point bending test set-up (left) and failure mode (right)**

## 2.2 Geometry of the tested hybrid beams and testing set-up measurements

Each hybrid beam was composed of an IPE 160 of steel grade S275 associated with two timber beams inserted between the steel beam flanges. Three configurations were tested including symmetrical and unsymmetrical steel cross-section: (I) with the full IPE, (II) the lower flange (tensile zone) of the IPE is cut, (III) the upper flange (compressive zone) of the IPE is cut. The two last configurations correspond to tee cross-sections which are characterized by similar geometries but different behaviours. In configuration (II), the steel section can reach plastic strength whereas for configuration (III), the compressed web panel is more sensitive to local instabilities and should have a reduced bending strength. Figure 6 shows the cross-sections and the dimensions of the tested beams.

The timber beams were connected to the steel beam by means of bolts of 8 mm diameter on the web and by means of screws of 4 mm diameter on the flanges. The position of bolts and screws were chosen according to the spacing recommendations of Eurocode 5. In order to observe the influence of the fasteners spacing, two distributions of connectors were studied: short spacing ( $v1$ ) and long spacing ( $v2$ ). Figure 7 shows the location of the fasteners for the three tested beams.

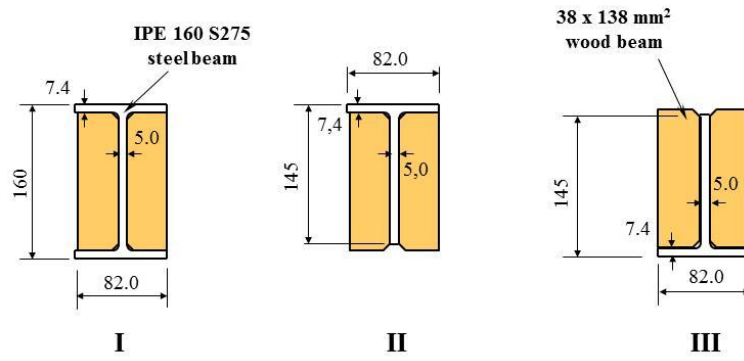


Figure 6: tested configurations of hybrid beams

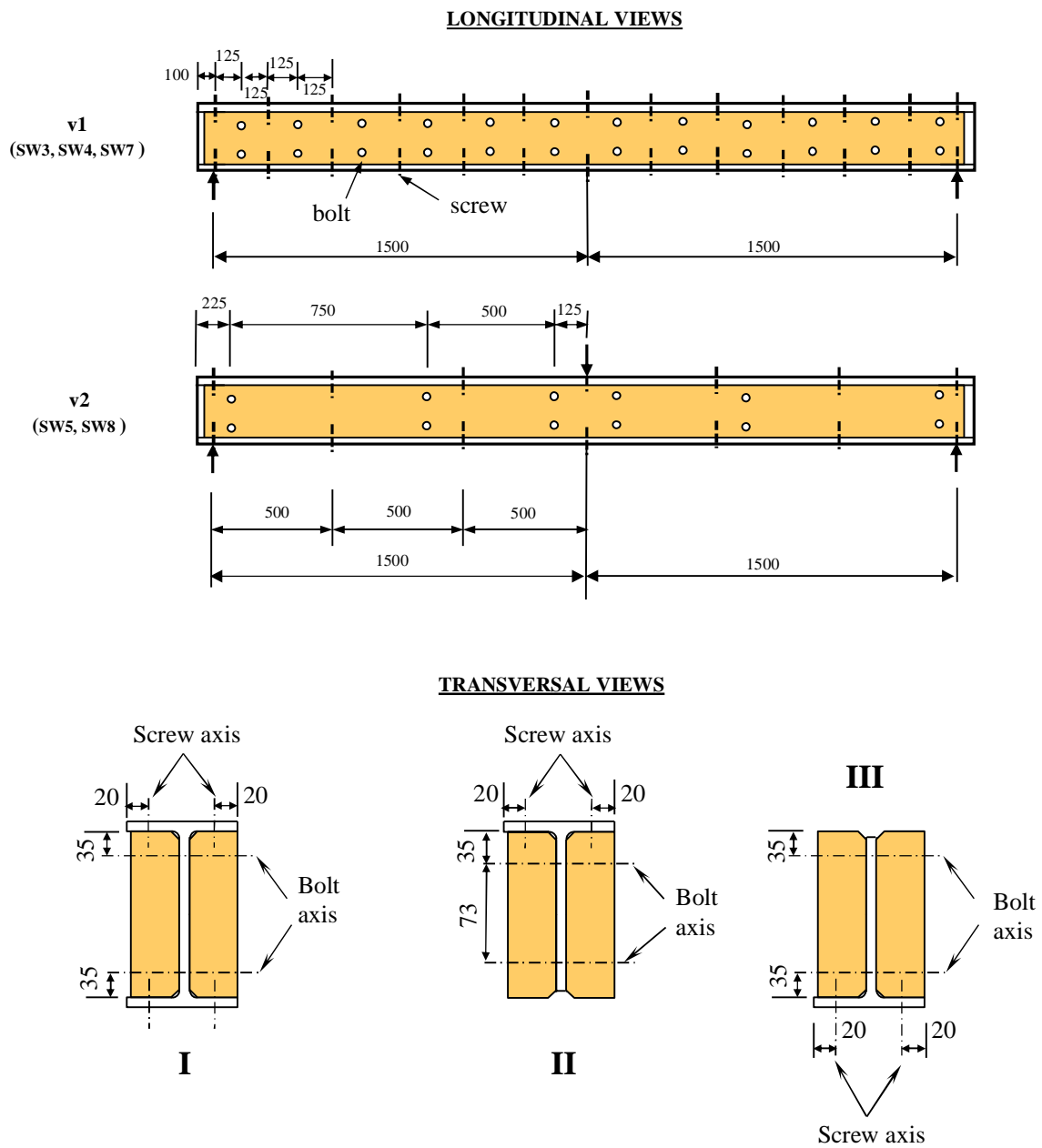


Figure 7: arrangements of bolts and screws to connect steel to timber beams

The tests were performed in two main steps. First, steel and timber beams were tested separately up to failure in 3-point bending with a span of 3 meters. The steel beams tested separately were similar to those used in the hybrid beams and were tested either with the load applied on the top (compression flange) or with the load applied on the bottom (tension flange). The load systems are shown in figure 8 for the full IPE steel beam (configuration (I)).

Timber beams, similar to those used in the hybrid beams, were also tested without steel beam (see figure 15).

In the second step, hybrid beams were tested up to failure in the same configuration as the separated elements. Table 1 gives a summary of all the tested beams (wood, steel and hybrid). One sample was tested for each configuration.

All specimens were loaded in 3-point bending with a span of 3 meters. The load was applied by hydraulic jack equipped with a spherical head connected to the tested beam by means of 3 elements: from top to bottom, a hemispherical steel cup, a steel transfer girder and a steel wedge element (Figure 9). The hemispherical cup was connected to the transfer girder allowing its partial rotation and therefore this of the tested beam with respect to the jack. Thus, the set-up allowed the initiation of lateral torsional buckling but provided some restrain for larger displacements. At the end supports, the vertical displacement  $U_z$ , the lateral displacement  $U_y$ , the rotation around x-axis and the rotation around z-axis were restrained (see Figure 9).

For all the tested beams, the load was increased up to failure with a loading rate of 4 mm/min. During the tests, the applied load, the mid-span deflection and the strains are measured with a frequency of 2 Hz. Several strain gauges are arranged along the beams length to measure the strains on steel and timber parts. Figure 9 shows the loading system and examples of the strain gauges positions.

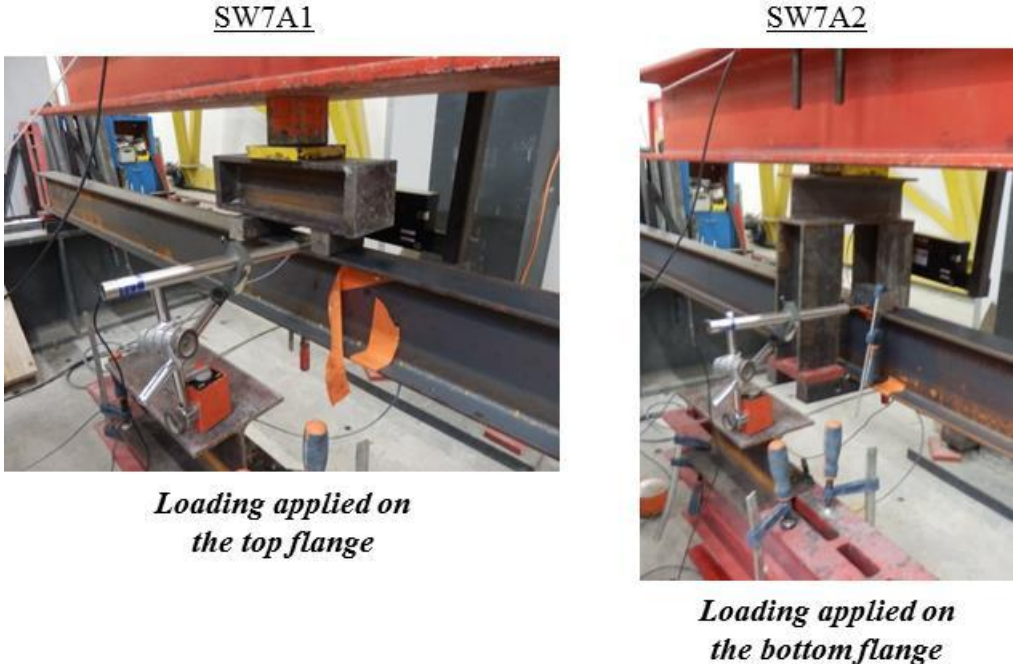
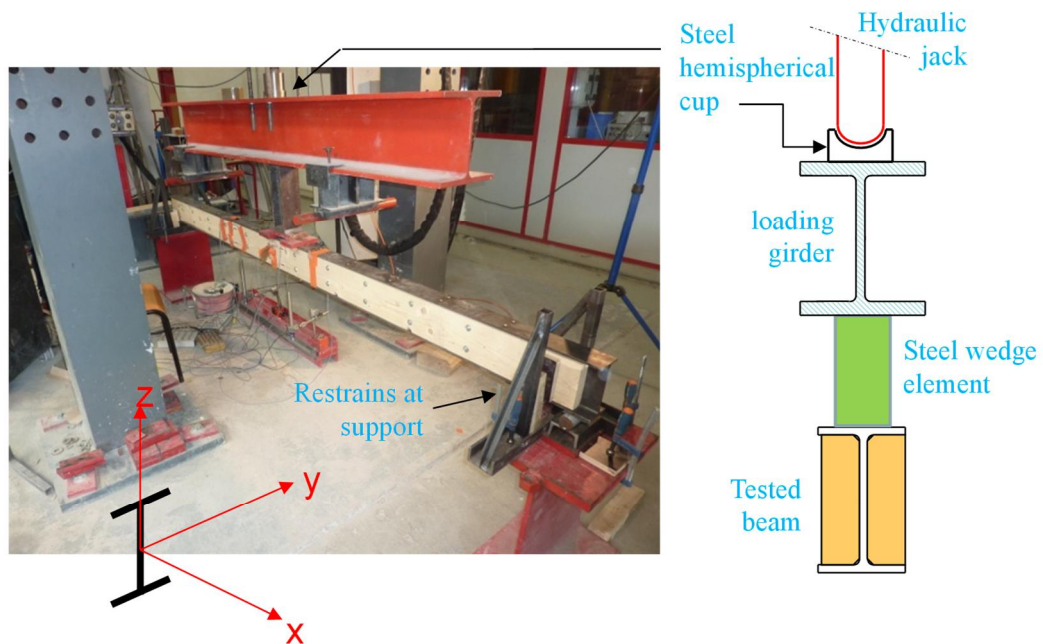


**Figure 8: loading devices of the steel beams SW7A1 and SW7A2**

### Supports and loading system



### Gauges location at mid-span

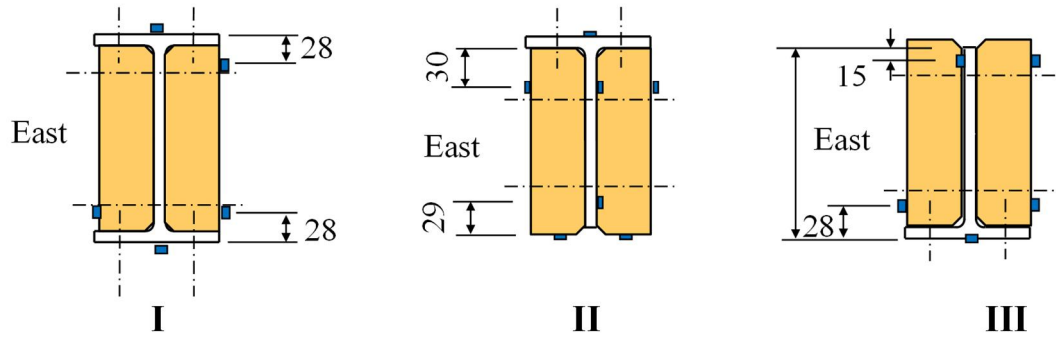


Figure 9: experimental set-up and strain gauges locations

Configurations		Steel beams	Wood beams	Hybrid beams	
				Arrangement v1	Arrangement v2
I		SW7A1 SW7A2	SW4B	SW7	SW8
II		SW9A		SW3	-
III		SW4A		SW4	SW5

Table 1: overview of the tested beams

### 3 Experimental results and discussions

#### 3.1 Materials properties

Figure 10 shows the results of tensile test performed on steel coupons. The mean values of the yield and ultimate limit obtained from the 3 specimens are equal to  $329.9 \pm 9.0$  MPa and  $462.0 \pm 4.2$  MPa respectively.

The mean value of moisture content in wood specimens was equal to  $9.2 \% \pm 0.7 \%$ . Small variation may be attributed to the variation of density or to the presence of knots. The same methodology has been used to obtain the wood density with a mean value of  $465.2 \text{ kg/m}^3$  and a coefficient of variation of  $15.4 \%$ .

Table 2 provides the main results of the elastic modulus and the wood strength obtained from bending tests for specimens with or without knots. The average elastic modulus and the average bending strength were about  $12.9 \text{ GPa}$  and  $82.4 \text{ MPa}$  respectively. The results presented in table 2 show that the presence of knots reduced the modulus of elasticity and the strength.

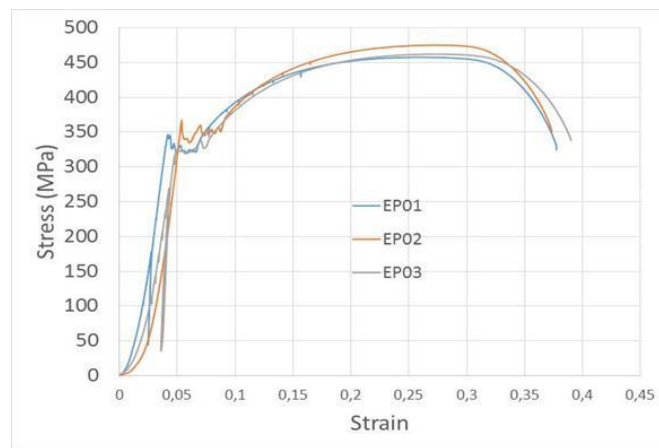


**Figure 10: stress-strain curves of steel on coupon tensile tests**

	<b>Local Modulus</b> (MPa)	<b>Global Modulus</b> (MPa)	<b>Ultimate bending stress</b> (MPa)
<b>Without knots</b>	$13953 \pm 4725$	$14425 \pm 6877$	$88.8 \pm 21.3$
<b>With knots</b>	$11517 \pm 3509$	$10379 \pm 4480$	$71.0 \pm 34.0$
<b>All results</b>	$12881 \pm 3426$	$12884 \pm 5109$	$82.4 \pm 26.9$

**Table 2: modulus of elasticity and tensile bending strength**

#### 3.2 Full scale bending behavior

##### 3.2.1 Steel beams

Two beams were tested for the full IPE steel beam (configuration (I)): beam SW7A1 with the load applied on the top (compression flange) and beam SW7A2 with the load applied at the bottom (tension flange). The load-displacement curves are provided in figures 11 and 12. It can be observed an acceleration of the lateral displacement for a load of about  $40 \text{ kN}$  whereas the maximum measured strain was about  $1.3 \%$ . As the yield limit strain of steel is evaluated at  $1.6 \%$  (assuming  $E_s = 210 \text{ GPa}$ ), it can be concluded that the beginning of non-linear behavior of the steel beam is due to lateral

buckling. Then, with the increase of load, yielding progressed and lateral displacement increased. The failure was reached by plastic deformation associated to lateral torsional buckling for a load close to 60 kN. Actually, this value is higher than the calculated elastic moment  $M_{el}$  of the cross-section (equal to 36 kN.m) that corresponds to a maximum load of 48 kN. Thus, the ultimate load of both I-beams was reached by plastic deformation combined with lateral torsional buckling. Consequently, the load position (top or bottom flange) seems to have no significant influence on the load carrying capacity of the beam. However, it can be observed in figure 12 that the failure was reached with a longer plastic plateau for the beam loaded on the bottom flange: in that last case, the cross-section seems to be more yielded.

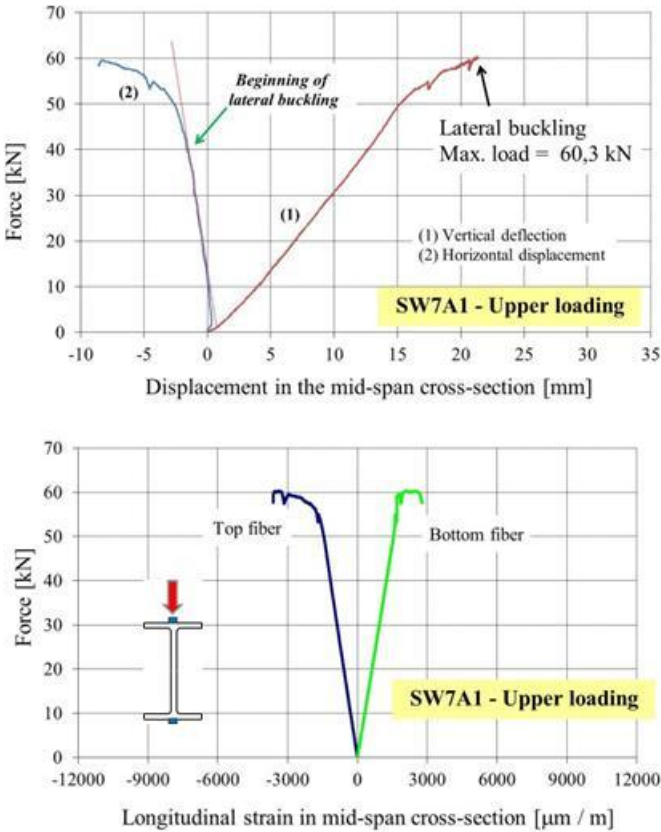


Figure 11: behavior of beam SW7A1 (configuration I)

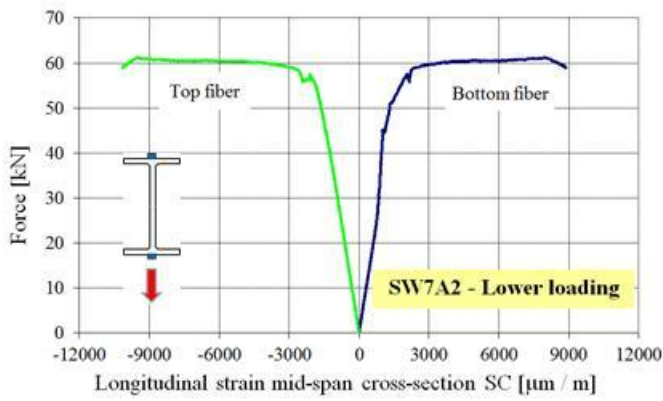
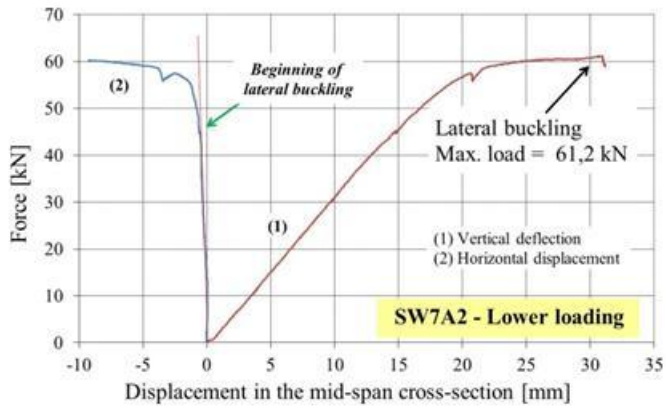


Figure 12: behavior of steel beam SW7A2 (configuration I)

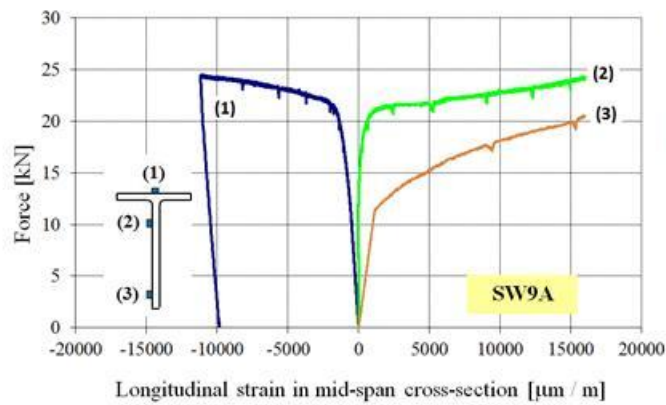
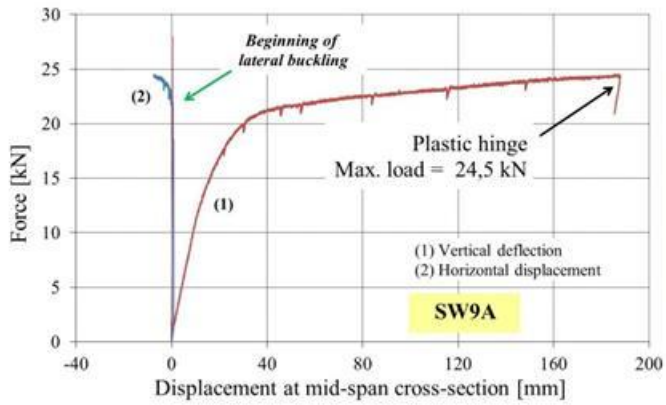


Figure 13: behavior of steel beam SW9A (configuration II)

The behavior of the steel beams with a tee section (configurations (II) and (III)), shown in figures 13 and 14, exhibited different failure modes. In the case of configuration (II) with the web panel in tension (beam SW9A), the failure was reached for a maximum load of 24.5 kN with high strains after a significant nonlinear part on the load-displacement curve. The high values given by the strain gauges located on the steel section (see figure 13) confirm the formation of a plastic hinge in the steel section at mid-span.

For configuration (III) with the flange in the tension zone (beam SW4A) and the web panel mostly in compression, the failure was reached by local buckling of the web for a maximum load equal to 19.4 kN. This local buckling was combined with a lateral torsional buckling of the whole beam. At failure, the strains remained relatively low, only the upper area of the cross section exhibited yielding

**3.2.2 Timber beams**

The behavior of timber beam SW4B is shown in figure 15. The failure was obtained by fracture in tension for a maximum load of 17.2 kN that corresponds to a maximum bending tensile stress of 54 MPa (evaluated from the maximum load and the moment of inertia). The modulus of elasticity obtained from bending tests was evaluated from the displacement measurement neglecting the shear effect and was about 10.5 GPa. This value is consistent with the modulus of elasticity measured on small knot free specimens according to specified rules for the determination of mechanical characteristics of timber [27].

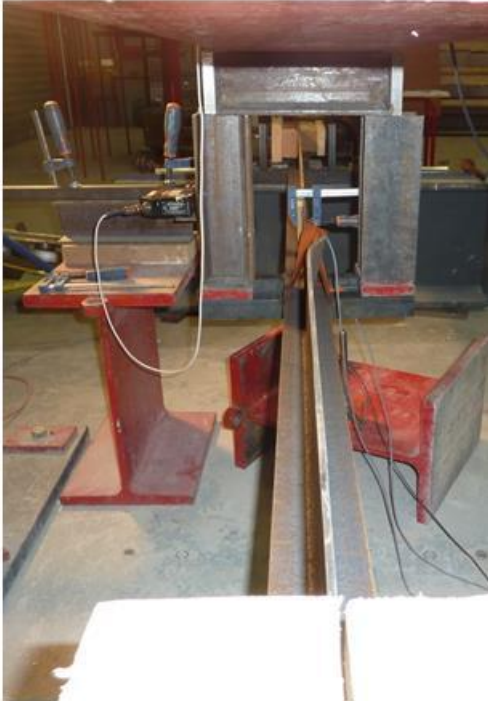
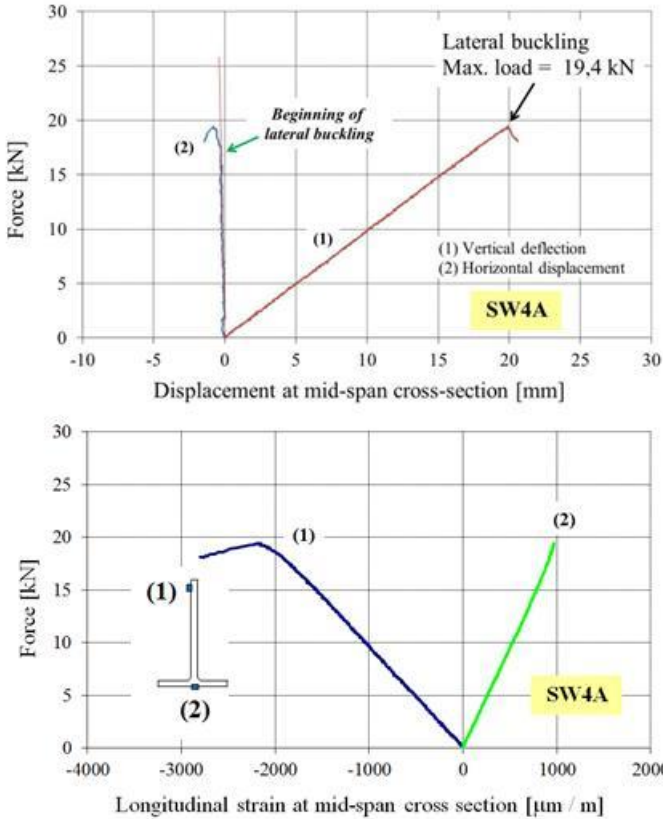


**Figure 14: behavior of steel beam SW4A (configuration III)**

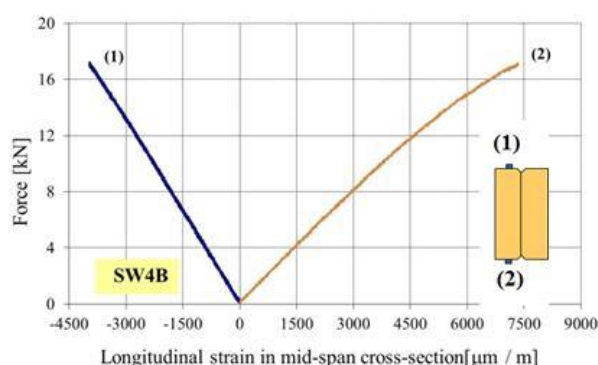
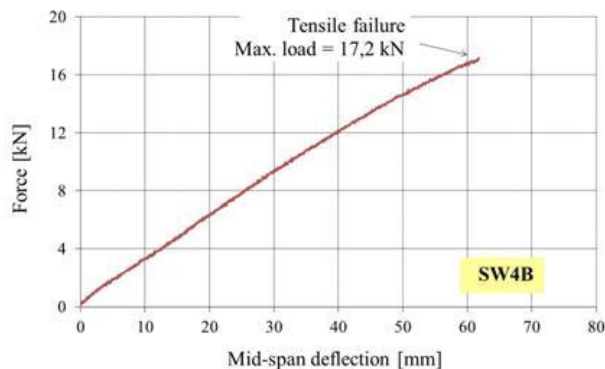


**Figure 15: experimental setup with load-displacement and load-strain curves of beam SW4B**

### 3.2.3 Hybrid beams

The loading was applied on the top of the beam for the configurations (I) and (II) and on the bottom for the configuration (III).

#### 3.2.3.1 Influence of the geometry

The behavior of hybrid beams is shown in Figures 16 to 18 for the 3 configurations I to III with the connectors spacing ( $v_1$ ). For the specimen SW7 (configuration (I)), it can be observed the linear evolution of the load-deflection and load-strain curves up to a load of about 48 kN. At this load, the strains are lower than 1.5 ‰ in the steel part and lower than 0.8 ‰ in the wood part confirming that both materials remain in the elastic stage. After that, the load-displacement curves become nonlinear up to a maximum load of about 62 kN corresponding to a failure by lateral torsional buckling at the central zone with high plastic deformations of the steel profile. Moreover, it can be observed that the value obtained from the strain gauge 3 in timber changes its sign (from tension to compression) close to the maximum load (figure 16). This can be explained by the lateral torsional buckling that created out of plane bending in the timber beam.

For the specimen SW3 (configuration (II)), the evolutions of the load-deflection and load-strain curves are linear up to a load close to 23 kN (figure 17). The strains at the top of mid-span cross-section are equal to -0.9 ‰ in steel and -0.4 ‰ in timber while these values are equal to 1.5 ‰ in steel and timber at the bottom fiber. Beyond the load of 23 kN, deflections and strains evolutions become nonlinear. The maximum load reached at about 45 kN coincides with longitudinal cracks in the two timber beams confirming shear failure in timber elements. After the test, the beam was disassembled and it has been observed important plastic strains in tension on the lower part of the steel tee web showing that the tearing of the web was imminent (see figure 17).

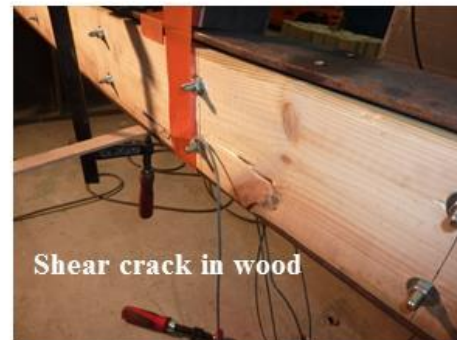
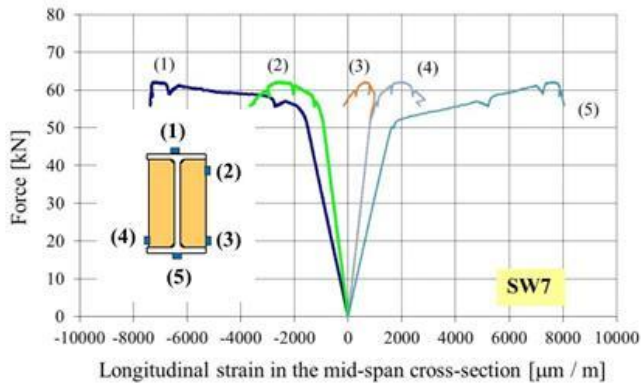
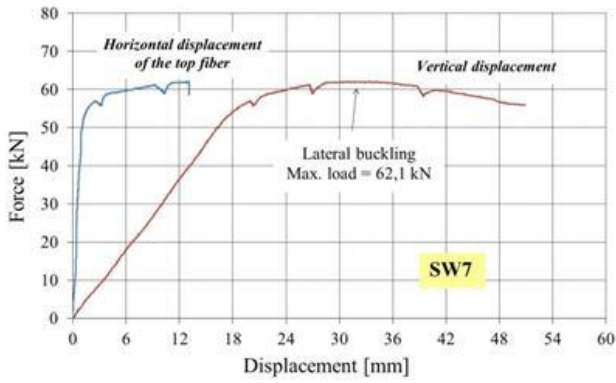


Figure 16: behavior of beam SW7 (configuration I – arrangement v1)

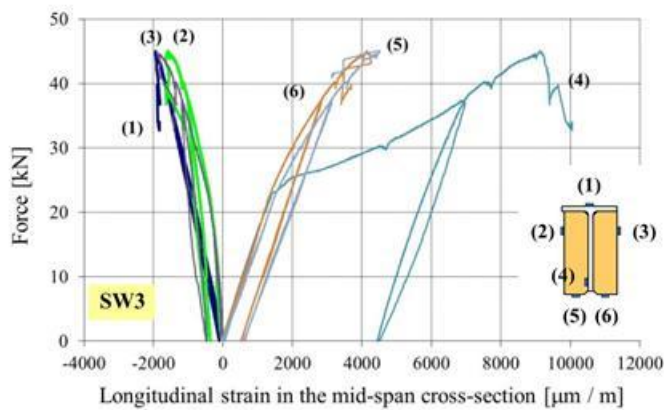


Figure 17: behavior of beam SW3 (configuration II – arrangement v1)

For the specimen SW4 (configuration (III)), the evolution of the load-deflection and the load-strain curves are linear up to about 20 kN (figure 18). At this load, the measured strains do not exceed 1.5 ‰ in all materials. Beyond this value, the load-displacement curve becomes highly nonlinear up to a maximal load of 36.3 kN. This value corresponds to the failure of the beam by local buckling of the steel web that « pushed-out » the adjacent wood elements creating thus out of plane bending. The out of plane bending due to the local buckling of the steel part has induced some cracks in the timber elements. At failure, the steel profile shows high plastic deformations in the bottom fiber and the measured strains on the timber element reached 2.6 ‰ in compression and 1.2 ‰ to 2.9 ‰ in tension (for the two timber beams observed). It can also be observed, that the timber and steel elements behaved as a composite cross-section with full connection until the local buckling started. As expected, the unsymmetrical shape can be observed on the measured strains between the top and the bottom of the section. Furthermore, even locally broken, the timber elements performed an efficient lateral support for the steel element, before and beyond the maximum load, allowing a significant structural ductility. Indeed, after the cracks observed in timber elements, the applied load dropped to about 24 kN and kept this value during a significant plateau. It can be observed that this value is close to the maximum load of the steel beam alone (see behavior of SW9A), meaning that the timber, even after several cracks, maintains the full plastic hinge capacity of the steel section.

From these experimental results, it can be observed that the behavior and the failure mode of the steel and hybrid beams confirmed that the contribution of the timber elements depends on the steel beam geometry and can provide significant additional strength and ductility.

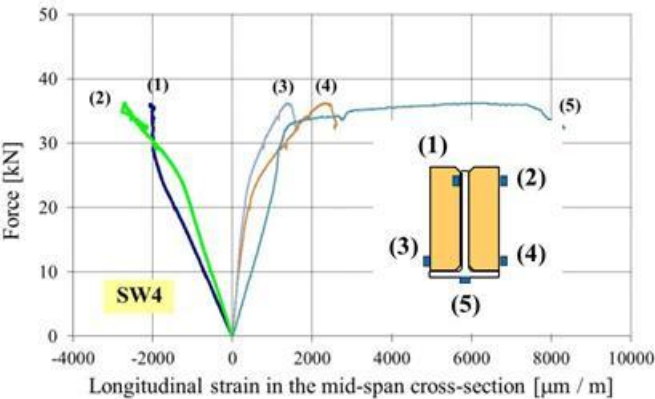
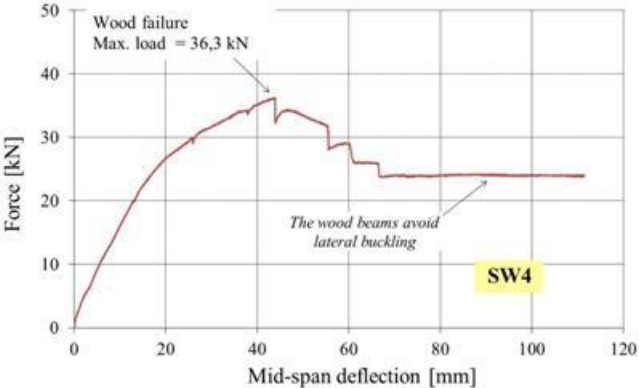


Figure 18: behavior of beam SW4 (configuration III – arrangement v1)

### 3.2.3.2 Influence of the connector's density

For the configuration (I) (I beam), the comparison between the specimens SW7 and SW8, that differed only by the density of connectors, is shown in figure 19. It can be observed that the failure mode does not change (plastic deformation with lateral torsional buckling) and that the difference of maximum loads is lower than 4 %. The differences are slightly higher for the mid-span deflections (7 % at 50 kN) and for the strains measured at the top of the timber beam (32 % at 50 kN). For the configuration (III) (tee steel section with flange at the bottom), the comparison between the specimens SW4 and SW5 (see figure 20) shows similar results as SW7 / SW8: the failure mode does not change (plastic deformation and local buckling) and the difference between the maximum loads is about 4 %. The differences are higher for the strains measured on the timber beam (43 % at 30 kN on the top of the beam).

These results show that the two densities of connectors tested (named v1 and v2) seem to have no significant influence on the behavior of the tested hybrid beams. Local effects of the bolts and the knots can explain the deviations observed in the measured value of strain in timber elements. However, further studies should confirm these results for several other bolts density and for various locations of connectors.

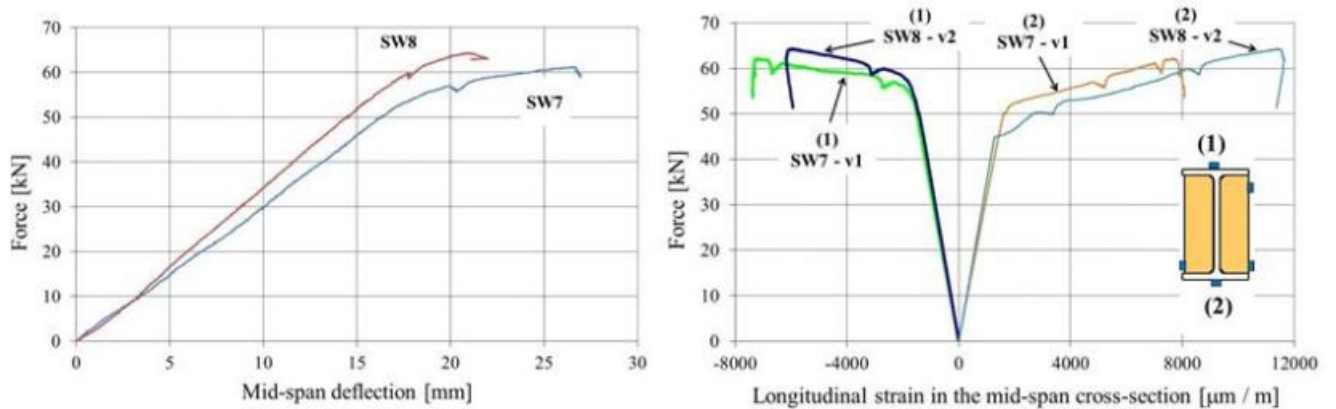


Figure 19: comparison between SW7 and SW8 (configuration I – arrangements v1 and v2)

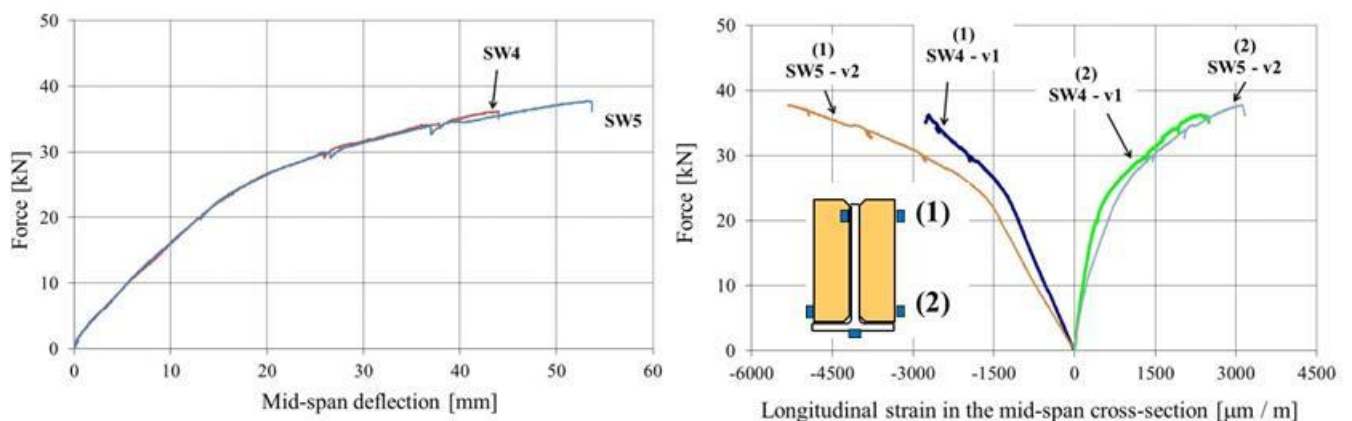


Figure 20: comparison between SW4 and SW5 (configuration III – arrangements v1 and v2)

### 3.2.3.3 Contribution of the composite action

The comparison between the hybrid elements and their basic components illustrated for each configuration, with the connectors' density  $v1$ , are shown in the figures 21 to 23 and in Table 3. For configuration (I) (I beam), the wood contribution to steel profile performances was low, both in the elastic domain and at failure (figure 21). The behavior of the hybrid beam was close to that of the steel alone. The ultimate load was increased by 3 % only and the failure mode remained the lateral torsional buckling. However, the hybrid element shows a ductile behavior with significant plastic plateau.

In the case of configuration (II) (tee with the flange in the compression zone), the contribution of wood to steel performances was very high (figure 22). In the elastic phase, the addition of wood increased significantly the stiffness of the steel beam. In addition, the failure mode changed with an increase of the maximum load by about 84 % with respect to steel beam only. Hence, the hybrid element, in spite of a succession of local fractures of wood, maintained a high level of ductility with a high residual strength.

In configuration (III) (tee with the flange in the tensile zone), the wood contribution to steel performances was also very high (figure 23). In the elastic phase, the addition of wood increased significantly the stiffness of the steel beam. The wood element provided a lateral support for the steel web increasing thus its resistance to lateral torsional buckling and local buckling. Actually, a plastic hinge could be reached at failure with an increase of the steel beam strength of about 87 %.

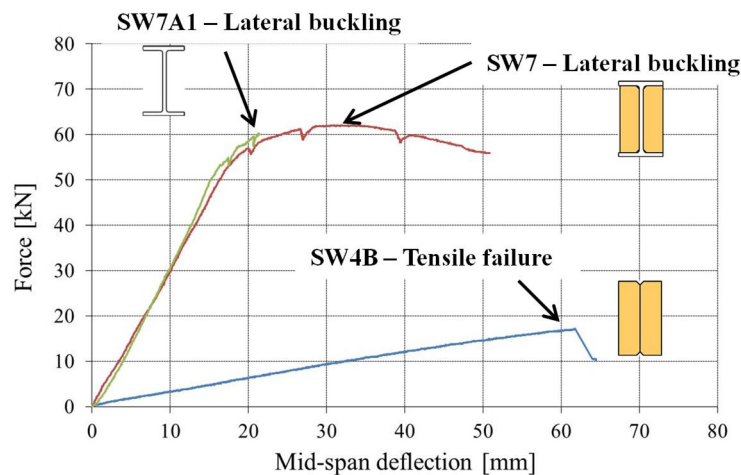


Figure 21: comparison between SW7, SW4B and SW7A1 (configuration I - arrangement  $v1$ )

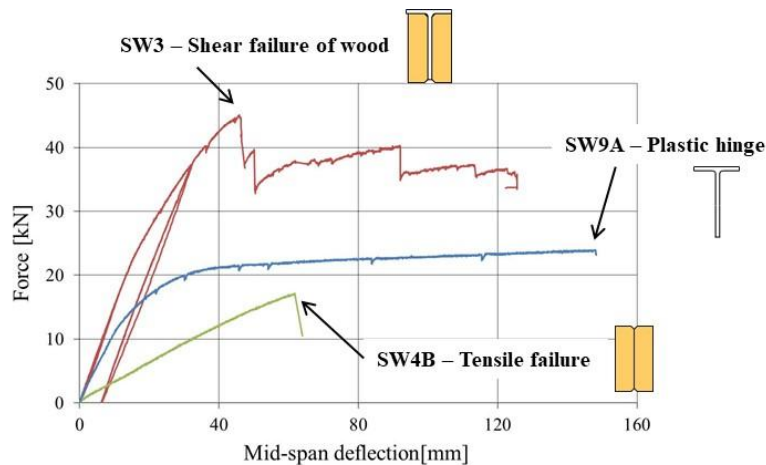


Figure 22: comparison between SW3, SW4B and SW9A (configuration II - arrangement  $v1$ )

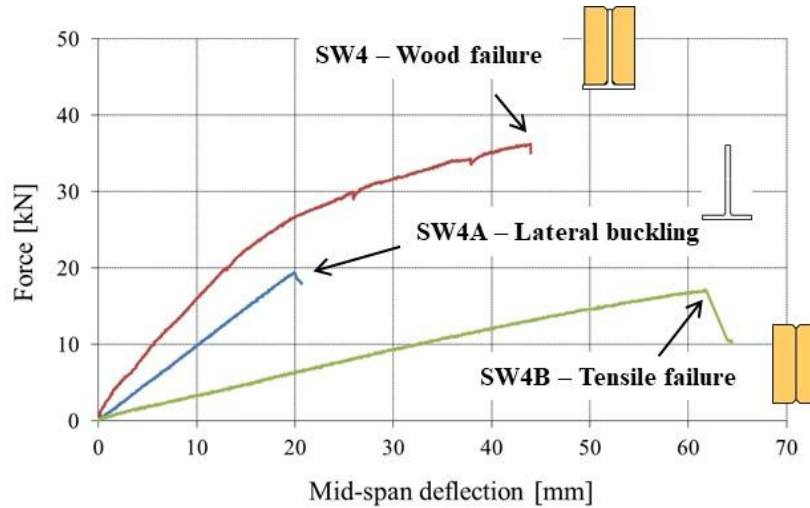


Figure 23: comparison between SW4, SW4B and SW4A (configuration III - arrangement v1)

		Elastic domain		Failure	
		$\frac{w_{\text{hybrid}}}{w_{\text{wood}}}$	$\frac{w_{\text{hybrid}}}{w_{\text{steel}}}$	$\frac{F_{\text{hybrid}} - F_{\text{wood}}}{F_{\text{wood}}}$	$\frac{F_{\text{hybrid}} - F_{\text{steel}}}{F_{\text{steel}}}$
I		11 %	93 %	+ 267 %	+ 3 %
II		22 %	70 %	+ 161 %	+ 84 %
III		20 %	63 %	+ 111 %	+ 87 %

$w$ : deflection at mid-span in the elastic domain  
 $F$ : failure load

Table 3: mechanical performance of hybrid beams compared to that of steel and wood beams

#### 4 Analytical modeling of the hybrid beam behavior

The analytical modeling concerns the initial elastic stage of behavior and the load carrying capacity. The results obtained by the analytical approaches are compared with those obtained from tests.

##### 4.1 Elastic stage

All the beams are modeled in the elastic stage using the analytical approach of Euler-Bernoulli beam theory. For the hybrid beam, a full connection is assumed between the steel and wood parts. Thus, the cross-section is homogenized using as reference steel in a similar way with steel-concrete composite beams [28]. The strain at each fiber can be deduced from stress using Hooke's law. In the present case, as the structure was tested on a 3-point bending over a simply supported span  $L$ , the vertical deflection at mid-span  $v(L/2)$  can be calculated as follows:

$$v_{\text{C}} = \frac{FL^3}{48 E_s I_{\text{hom}}} + \frac{FL}{4 G_s W_{\text{Vhom}}} \quad (1)$$

F is the applied load,  $E_s$  and  $G_s$  are the elastic modulus and the in-plane shear modulus of the steel profile respectively,  $I_{\text{hom}}$  is the inertia of the homogenized section and  $W_{\text{hom}}$  is its shear area evaluated by means of the following equation:

$$\Omega_{V_{\text{hom}}} = \Omega_{V_s} + \frac{G_w}{G_s} \cdot \frac{5}{6} \cdot \Omega_w \quad (2)$$

$G_w$  is the in-plane shear modulus of the wood beam,  $W_w$  is the area of the timber beam,  $W_{V_s}$  is the shear area of the steel profile. For IPE beams, it may be admitted that the main contribution to shear is due to the web panel of the steel profile. Therefore in Eq. (2),  $W_{V_s}$  may be substituted by the web area  $W_{\text{web}}$  of the steel profile.

The material and geometric characteristics of homogeneous and hybrid cross-section are summarized in table 4. For each beam in the elastic stage, the mid-span deflection and the stresses at different positions along the cross-section are calculated and compared to the experimental values in table 5.

	$E_s$ GPa	$G_s^{(5)}$ GPa	$E_w$ GPa	$G_w^{(6)}$ GPa	$y_G^{(1)(3)(4)}$ mm	$\Omega^{(3)(4)}$ mm <sup>2</sup>	$\Omega_V^{(3)(4)}$ mm <sup>2</sup>	$I^{(2)(3)(4)} \times 10^6$ mm <sup>4</sup>
SW7A	210	80.8	-	-	80.0	2010	800	8.69
SW9A	210	80.8	-	-	42.2	1295	725	2.78
SW4A	210	80.8	-	-	102.8	1295	725	2.78
SW4B	-	-	12.9	0.5	69.0	10488	8740	16.6
SW7	210	80.8	12.9	0.5	80.0	2650	854	9.7
SW3	210	80.8	12.9	0.5	53.5	1935	779	4.1
SW4	210	80.8	12.9	0.5	91.9	1935	779	4.1

(1) with respect to the top fiber

(2) with respect to the neutral axis

(3) round corner neglected for the tee beams

(4) homogenised properties in the case of hybrid beam

(5)  $G_s = E_s / (2(1 + \nu))$ ,  $\nu = 0.3$

(6)  $G_w$  provided by Eurocode 5

Equations used in the case of hybrid beams SW3, SW4 and SW7 :

$$y_{G_{\text{hom}}} = \frac{y_{G_s} \times \Omega_s + n \times y_{G_w} \times \Omega_w}{\Omega_s + n \times \Omega_w} \quad \Omega_{\text{hom}} = \Omega_s + n \times \Omega_w \quad I_{\text{hom}} = I_s + n \times I_w \quad n = \frac{E_w}{E_s}$$

**Table 4: material and geometric properties used in the model**

Configurations	F	V (L/2)			Fiber (1)				Fiber (2)				Fiber (3)			
		$v^{th}$	$v^{exp}$	Diff.	$\sigma_{th}$	$\epsilon_{th}$	$\epsilon_{exp}$	Diff.	$\sigma_{th}$	$\epsilon_{th}$	$\epsilon_{exp}$	Diff.	$\sigma_{th}$	$\epsilon_{th}$	$\epsilon_{exp}$	Diff.
		kN	mm	mm	%	MPa	$\mu\text{m/m}$	$\mu\text{m/m}$	%	MPa	$\mu\text{m/m}$	$\mu\text{m/m}$	%	MPa	$\mu\text{m/m}$	$\mu\text{m/m}$
SW7A	30	9.6	10.0	4.0	-207.1	-986	-890	10.8	207.1	986	845	16.7	-	-	-	-
SW9A	10	9.0	8.8	2.3	-113.8	-542	-492	10.2	219	1043	982	6.2	-	-	-	-
SW4A	10	9.0	10.0	10.0	-236.9	-1128	-1028	9.7	113.8	542	480	12.9	-	-	-	-
SW4B	10	27.2	32.2	15.5	-31.1	-2411	-2190	10.1	31.1	2411	3638	33.7	-	-	-	-
SW7	40	11.5	13.0	11.5	-247.4	-1178	-1198	1.7	-9.8	-760	-710	7.0	247.4	1178	1254	6.1
SW3	20	13.6	13.2	3.0	-195.7	-932	-766	21.7	-3.6	-281	-330	14.8	261.6	1246	1202	3.7
SW4	15	10.2	9.6	6.2	-186.3	-887	-1064	16.6	-11.4	-891	-802	11.1	146.8	699	708	1.3

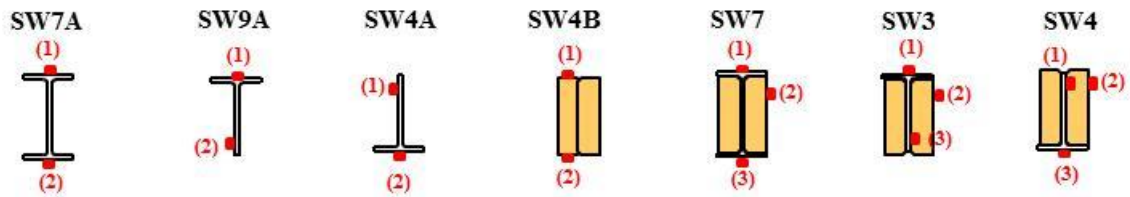


**Table 5: deflection, strain and stress in the elastic domain (analytical and experimental results)**

For the steel beam specimens (SW7A, SW9A, SW4A), the differences between the measured and calculated values are lower than 10 % (except for two strain values). For the wood beam SW4B, the discrepancies are unsurprisingly greater as the modulus of elasticity used in the calculation and the strains measured strongly depend on the variability of local conditions such as the numerous knots present in the beam. Actually, the calculated value is based on the modulus of elasticity obtained from the knot free small specimens ( $E_w = 12.9$  GPa), with a length lower than 900 mm, tested in bending (see sections 2.1 and 3.1). Thus, the difference can be explained partly by the presence of numerous knots in the full-scale beam.

In the case of hybrid beams (SW3, SW4, SW7), the differences between the measured and calculated values vary between 1.3 % and 21.7 %. Regarding the measured strains on wood and steel elements, these discrepancies can be considered as acceptable. The discrepancies relative to strains may be explained by the presence of knots but also by local effects of fasteners.

In the frame of this study, the simple Euler-Bernoulli beam theory allows to predict with an acceptable accuracy the global and the local responses of steel-timber hybrid structures within the elastic range.

## 4.2 Ultimate load

The analysis of ultimate strength is performed considering the steel beam and the hybrid beam combining steel and wood.

### 4.2.1 Steel beams ultimate loads

The analytical model is based on the European standard EN 1993-1-1 [29] and the elastic critical moment for lateral-torsional buckling  $M_{cr}$  obtained from the software LTbeam [30]. In the analysis, the ultimate loads  $F_{el,Rd}$  and  $F_{pl,Rd}$  are based on the elastic and the plastic moment of the steel profile,  $F_{eff,Rd}$  is the reduced ultimate load taking into account the reduction of moment due to local buckling and  $F_{LT,Rd}$  is the ultimate load considering the lateral torsional buckling of the beam. The maximum effect is considered at the mid-span of the beam. For each case, based on tensile tests results (see §3.1), the yield strength is assumed to be equal to  $f_y = 330$  MPa.

In order to represent the testing conditions, the vertical displacement  $U_z$ , the lateral displacement  $U_y$ , the rotation around x-axis and the rotation around z-axis were restrained at the end supports (see reference axis in Table 6). In addition, at mid-span, the lateral displacement  $U_y$ , the rotation around x-axis and the rotation around z-axis were restrained assuming that the loading system didn't allow free movement of the beam.

For the configuration (I), the IPE profile is of class 1 and its corresponding ultimate load is  $F_{pl,Rd} = 54.5$  kN. However, the global strength can be limited by lateral torsional buckling. The critical elastic moment is  $M_{cr} = 143.2$  kN.m. Thus, the ultimate load taking into account the lateral torsional buckling is  $F_{LT,Rd} = 46.8$  kN (reduction factor  $c_{LT} = 0.859$ ). This value is lower than the experimental one ( $F_u$  test  $\approx 60$  kN). It can be observed in figures 11 and 12 (specimens SW7A1 and SW7A2) that the nonlinear phase of the load-deflection curve begins for a load between 40 and 50 kN which corresponds to the beginning of the lateral torsional buckling phenomenon.

For the configurations (II) and (III), the tee section was obtained from the IPE profile on which one flange has been removed. According to EN 1993-1-1, the flange is of class 1 [29] whereas the web is either of class 1 for configuration (II) (tee flange in compression) or of class 4 for configuration (III) (tee flange in tension). In configuration (III), the effective area has to be considered to take into account local buckling of the web panel.

The plastic and elastic ultimate load are respectively equal to  $F_{pl,Rd} = 23.8$  kN and  $F_{el,Rd} = 13.2$  kN. As the cross-section is of class 4 in configuration (III), the effective cross-section is calculated leading to the reduced ultimate load  $F_{eff,Rd} = 8.1$  kN.

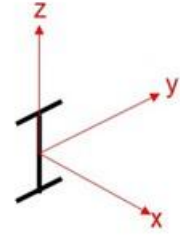
Regarding the torsional buckling, the elastic critical moment is equal to  $M_{cr} = 131.0$  kN.m (configuration II) and  $M_{cr} = 17.5$  kN.m (configuration III). These critical moments are calculated considering the full cross-section and not the effective one as recommended in EN 1993-1-1. The difference is due to the position of the flange in compressed or tensile zone [29].

In configuration (II) where the maximum compressive stress is in the flange, the tee section is of class 2 (beam SW9A). Thus, the ultimate load corresponds to  $F_{pl,Rd}$ . The ultimate load taking into account the lateral torsional buckling is  $F_{LT,Rd} = 22.4$  kN (reduction factor  $\chi_{LT} = 0.942$ ). This theoretical failure load is about 3 % lower than the experimental results (figure 13).

In the case of configuration (III), the ultimate load taking into account the lateral torsional buckling is  $F_{LT,Rd} = 5.8$  kN (reduction factor  $\chi_{LT} = 0.717$ ). This theoretical failure load is about 70 % lower than the experimental results (figure 14). Hence, the analytical ultimate load is very low compared to that obtained from tests. Furthermore, it can be noticed that the experimental failure load was between the elastic and the plastic loads obtained by analytical approach (see Table 7). This should mean that the tee section is close to a class 3 section rather a class 4 section. Eurocode design rules seems to be very conservative in the case of tee sections.

In order to appreciate the influence of boundary conditions on the prediction of the failure load  $F_{LT,Rd}$ , several theoretical boundary conditions are considered (see Table 6). The results confirm that the restrain of displacement along y-axis at mid-span has a great influence on the predicted failure load for each configuration. In addition, it appears that in the case of configuration (III), Eurocode design rules seem to be conservative for lateral torsional buckling of class 4 sections.

Boundary conditions at supports <sup>(1)</sup>	U <sub>z</sub> , U <sub>y</sub> , R <sub>x</sub>	U <sub>z</sub> , U <sub>y</sub> , R <sub>x</sub>	U <sub>z</sub> , U <sub>y</sub> , R <sub>x</sub>	U <sub>z</sub> , U <sub>y</sub> , R <sub>x</sub> , R <sub>z</sub>	U <sub>z</sub> , U <sub>y</sub> , R <sub>x</sub> , R <sub>z</sub>
Boundary conditions at mid-span <sup>(1)</sup>	no restraint	U <sub>y</sub>	U <sub>y</sub> , R <sub>x</sub>	U <sub>y</sub> , R <sub>x</sub>	U <sub>y</sub> , R <sub>x</sub> , R <sub>z</sub>
SW7.A1 	F <sub>u</sub> = 25.8 kN	F <sub>u</sub> = 42.3 kN	F <sub>u</sub> = 45.5 kN	F <sub>u</sub> = 46.8 kN	F <sub>u</sub> = 46.8 kN
SW7.A2 	F <sub>u</sub> = 34.8 kN	F <sub>u</sub> = 45.5 kN	F <sub>u</sub> = 45.5 kN	F <sub>u</sub> = 46.8 kN	F <sub>u</sub> = 51.1 kN
SW9.A 	F <sub>u</sub> = 15.3 kN	F <sub>u</sub> = 21.5 kN	F <sub>u</sub> = 21.5 kN	F <sub>u</sub> = 22.4 kN	F <sub>u</sub> = 23.8 kN
SW4.A 	F <sub>u</sub> = 5.5 kN	F <sub>u</sub> = 5.8 kN	F <sub>u</sub> = 5.8 kN	F <sub>u</sub> = 5.8 kN	F <sub>u</sub> = 5.8 kN



<sup>(1)</sup> U<sub>i</sub> = translation restrained along i-axis - R<sub>i</sub> = rotation restrained around i-axis

**Table 6: Influence of the boundary conditions on the predicted failure load**

#### 4.2.2 Hybrid beams ultimate loads

The maximum bending strength of the hybrid beam, named  $M_u^{\text{hyb}}$ , is calculated as the maximum capacity of the cross-section without any local buckling or lateral-torsional buckling. It can be evaluated from an original multi-layer model, similar to that used for steel-concrete composite beams [31-33], adapted to the case of timber-steel beams considering a full connection between the two materials. In addition, in the critical cross-section, it is considered that at failure, the steel profile reaches its plastic capacity and that the wood element remains elastic but reaches on the most loaded fiber its strain limit  $\epsilon_{w \text{ max}}$  or its stress limit  $\sigma_{w \text{ max}}$ .

In the case of cross-section with double symmetry (configuration (I) – beam SW7), as the centroid of timber and steel elements are in the same location, the moment  $M_u^{\text{hyb}}$  of the hybrid cross-section is the sum of the steel beam plastic moment  $M_{pl}^s$  and the wood beam elastic moment  $M_{el}^w$ . Assuming  $f_y = 330$  MPa and  $\sigma_{w \text{ max}} = 54$  MPa, it gives:

$$M_{pl}^s = Z_x \cdot f_y = 124 \cdot 10^{-6} \text{ m}^3 \cdot 330 \cdot 10^6 \text{ Pa} = 40.9 \text{ kNm} \quad (3)$$

$$M_{el}^w = \frac{bh^2}{6} \cdot \sigma_{w \text{ max}} = \frac{2 \cdot 0.038 \cdot (0.138)^2}{6} \text{ m}^3 \cdot 54 \cdot 10^6 \text{ Pa} = 13.0 \text{ kNm} \quad (4)$$

Thus, the maximum bending strength of the hybrid beam is equal to  $M_u^{\text{hyb}} = 53.9$  kNm and that corresponds to an ultimate load of  $F_{Rd} = 71.9$  kN.

In the case of unsymmetrical hybrid sections with steel tee and the flange on the compressive zone (configuration (II) – beam SW3), it is necessary to evaluate the position of the neutral plastic axis of the cross-section considering the equilibrium between compression force  $N_C$  and tension force  $N_T$  in the cross-section under bending. For the cross-section studied (see figure 24a), it gives:

$$N_C = N_C^w + N_{C1}^s + N_{C2}^s \quad (5)$$

$$N_T = N_T^w + N_T^s \quad (6)$$

$N_C^w$  is the compression force in the upper part of the wood beam,  $N_C^{s1}$  is the compression force in the upper part of the steel web,  $N_C^{s2}$  is the compression force in the top flange of the steel beam,  $N_T^w$  is the tension force in the lower part of the wood beam and  $N_T^s$  is the tension force in the lower part of the steel web. Each term in equations (5) and (6), described in figure 24a, is defined as follows:

$$N_C^w = 0.5 (y - t_f) b_w \sigma^{\text{sup}} = 0.5 (y - t_f) b_w E_w \varepsilon^{\text{sup}} \quad (7)$$

$$N_T^w = 0.5 (h_w + t_f - y) b_w \sigma_{w \text{max}} = 0.5 (h_w + t_f - y) b_w E_w \varepsilon_{w \text{max}} \quad (8)$$

$$N_T^s = f_y t_w (h_w + t_f - y) \quad (9)$$

$$N_{C1}^s = f_y t_w (y - t_f) \quad (10)$$

$$N_{C2}^s = f_y b t_f \quad (11)$$

In these equations,  $y$  is the distance between the top fiber of the cross-section and the plastic neutral axis,  $t_f$  the flange thickness,  $b$  the flange width,  $t_w$  the web thickness,  $h_w$  the web height which is equal to the wood beam height,  $b_w$  the wood beam width,  $f_y$  the steel yield limit and  $E_w$  the wood modulus of elasticity. The Navier-Bernouilli assumption induces:

$$\frac{\varepsilon^{\text{sup}}}{y - t_f} = \frac{\varepsilon_{w \text{max}}}{h_w + t_f - y} \quad (12)$$

Introducing equations (7) to (12) in equations (5) and (6) and considering that  $N_C = N_T$  leads to:

$$\alpha (y - t_f)^2 + \beta (y - t_f) + \gamma = 0 \quad (13)$$

with:

$$\alpha = 2 f_y t_w \quad (14)$$

$$\beta = f_y b t_f - 3 f_y t_w h_w - h_w b_w E_w \varepsilon_{w \text{max}} \quad (15)$$

$$\gamma = 0.5 h_w^2 b_w E_w \varepsilon_{w \text{max}} + f_y t_w h_w^2 - f_y b t_f h_w \quad (16)$$

Once  $y$  calculated, the maximum moment can be obtained by:

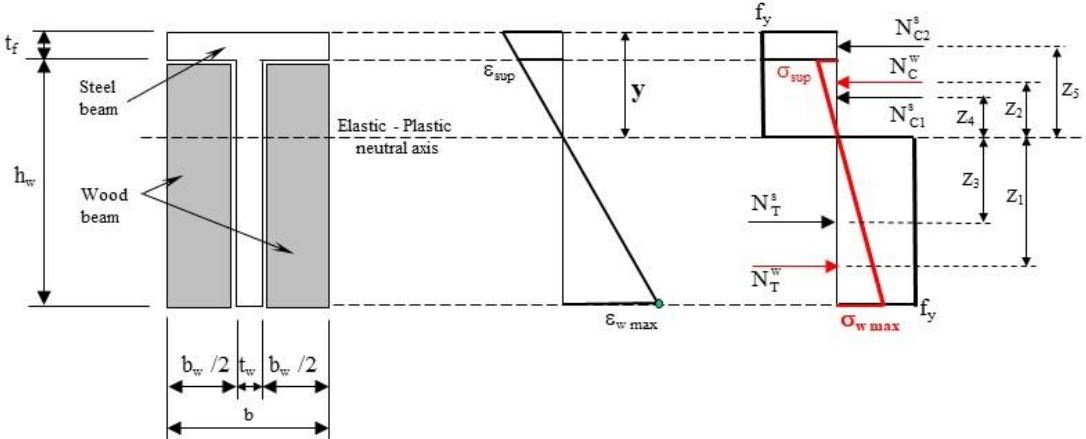
$$M_u^{\text{hyb}} = \sum_i \mathring{a}_i N_i \cdot Z_i \quad (17)$$

In this equation,  $N_i$  is the longitudinal force corresponding to the normal stress acting on the area  $i$  and  $Z_i$  is the distance between the resultant of stress and the plastic neutral axis of the cross-section (see details on figure 24a).

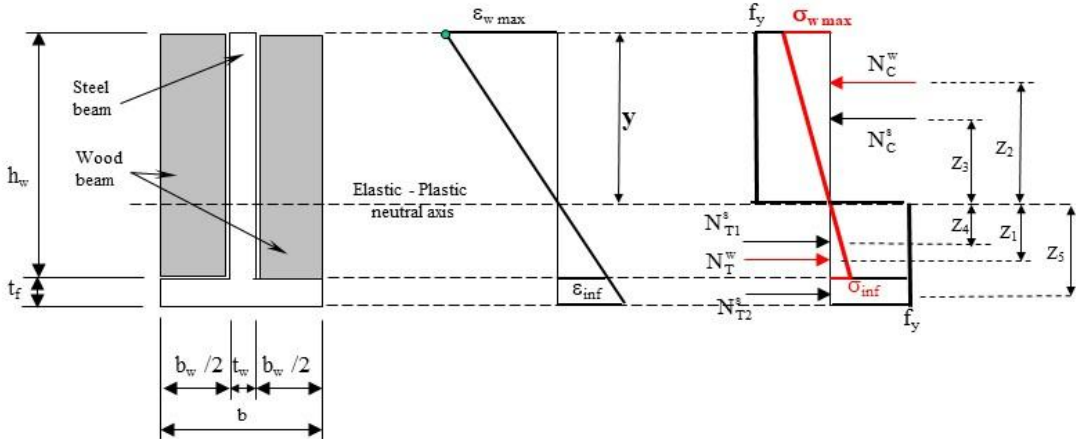
The bending strength of the hybrid sections with tee steel and the flange on the tensile zone (configuration (III) – beam SW4) is equal to that of the configuration (II) as the materials exhibit symmetrical behavior in tension and compression (figure 24b). Therefore, the previous equations may be used interchanging tension forces and compression force,  $e_{\text{sup}}$  and  $e_{\text{inf}}$ .

The calculated ultimate bending strength  $M_u^{hyb}$  is evaluated for SW3 et SW4 with the following assumptions: the maximum strain value of wood  $\epsilon_{w \max} = 0.007$  is taken from the full-scale tests in bending of wood beams (see figure 16) and its modulus of elasticity  $E_w = 12.9 \text{ GPa}$  is that obtained from small specimens in bending (see table 2). In the case of SW3 and SW4, the distance  $y$  between the top fiber of the cross-section and the plastic neutral obtained from equation (13) is  $y = 62.8 \text{ mm}$  which allows, using equation (17) to calculate the ultimate bending moment  $M_u^{hyb} = 40.3 \text{ kNm}$ . That corresponds to a failure load of  $F_{Rd} = 53.7 \text{ kN}$ .

The ultimate load  $F_{LTRd}$  of the hybrid beam considering the lateral torsional buckling is obtained from the calculated maximum bending strength  $M_u^{hyb}$ . This ultimate bending moment does not take into account the shear failure that occurred after the plastic hinge formation nor instabilities. As first approximation and conservative approach, the reduction factor  $\chi_{LT}$  of the steel beam is used. The ultimate loads corresponding to these resistant bending moments are compared to those given by tests (table 7).



(a) Configuration II (beam SW3)



(b) Configuration III (beam SW4)

**Figure 24: strain and stress diagrams in the hybrid beams**

For the specimen SW7, the ultimate load calculated neglecting the lateral-torsional buckling effect is equal to 71.9 kN while that calculated for steel beam (SW7A) is equal to 54.5 kN. The presence of

wood beams has a significant positive effect on the bending strength of the hybrid beam. Considering the lateral-torsional buckling and  $\chi_{LT} = 0.859$ , the calculated ultimate load of the specimen SW7 (configuration (I)) decreases to 61.8 kN which is close to the value obtained by tests (62 kN). The presence of wood beams delays slightly the lateral-torsional buckling for symmetrical hybrid beam. In that configuration, the interest of wood beams may be greater in the case of steel profile with thinner flanges and thinner web.

For the specimen SW3 (configuration (II)), the ultimate load calculated neglecting the lateral-torsional buckling effect is equal to 53.7 kN that is nearly twice that of the steel beam alone (SW9A) which is equal to 23.8 kN. The calculated failure load of the hybrid beam SW3 taking into account the global lateral buckling with  $\chi_{LT} = 0.942$  reached 50.6 kN which overestimated the measured failure load of about 12%. This discrepancy may be explained by the fact that the failure of SW3 was not only lateral-torsional buckling as web buckling took place.

In the case of the specimen SW4 (configuration (III)), the ultimate load calculated neglecting local buckling and lateral-torsional buckling effect was equal to 53.7 kN. The calculated failure load of the hybrid beam SW4 taking into account the global lateral buckling with  $\chi_{LT} = 0.717$  reached 38.5 kN which overestimated the measured failure load of about 6%. This discrepancy may be explained by the fact that the failure of SW4 was due to shear failure in wood beam and was not lateral-torsional buckling.

Moreover, it may be noticed that a variation of 10% on the value of  $\epsilon_{w \max}$  or  $E_w$  induces a variation of about 5 % on the value of  $M_u^{\text{hyb}}$  and also on the calculated ultimate load  $F_{LTRd}$ .

These different results show the relevance of the proposed approach. They also show that the proposed approach needs to be improved to predict more accurately the reduction factor of the lateral torsional-buckling of the hybrid beams combining steel and wood, especially if the response of the beam greatly depends on instability.

In the case of SW4. Indeed, for this specimen, the load was applied to the steel profile from bottom (on the flange) and the load transfer between steel and wood was performed only through bolts acting as local loads on the wood beam. In the other specimens (SW7 and SW3), the load was applied on the top of the steel beam. Thus, the load transfer between steel and wood mobilized the continuous contact between the two elements limiting thus the local transfer of load through bolts. This was not taken into account in the analytical model.

		Failure Load [kN]			
		Theory <sup>(1)</sup>			Test (failure mode)
		F <sub>Rd</sub>	$\chi_{LT}$ <sup>(2)</sup>	F <sub>LT,Rd</sub>	
SW7A1 (I)	I	54.5	0,859	46,8	60.3 (lateral buckling)
SW9A (II)	T	23.8	0,942	22,4	24.5 (plastic hinge)
SW4A (III)	L	7.7	0,717	5,8	19.4 (lateral buckling)
SW7 (I)	II	71.9	0,859	61,8	62.0 (lateral buckling)
SW3 (II)	II	53.7	0,942	50,6	45.1 (web buckling)
SW4 (III)	II	53.7	0,717	38,5	36.3 (shear failure in wood beam)

<sup>(1)</sup> : calculated assuming  $b = 82 \text{ mm}$ ,  $t_f = 7.4 \text{ mm}$ ,  $t_w = 5 \text{ mm}$ ,  $h_w = 138 \text{ mm}$ ,  $b_w = 76 \text{ mm}$ ,  $E_w = 12.9 \text{ GPa}$ ,  $f_y = 330 \text{ MPa}$ ,  $\epsilon_{maxw} = 0.007$

<sup>(2)</sup> : calculated from EC3 considering the steel beam only

**Table 7: Failure loads (analytical results versus test results)**

## 6 Conclusions

This paper presents the mechanical behavior of hybrid steel-timber beams connected by bolts and screws. The steel beams are usual IPE profiles but the wood beams are chosen from ungraded wood with numerous knots and defects, which are not usually used for structural applications. This preliminary study aims to demonstrate that, even with low quality wood elements, the hybrid beneficial effect can be mobilized in structural applications.

The characterization of materials highlighted the influence of the knots that tends to decrease, in a very important way in some cases, the modulus of elasticity and strength in comparison with the local measurement on defect-free specimens.

The hybrid beams were fabricated considering 3 different geometric configurations and 2 connectors' densities and they were tested in bending up to failure. The results show that the connectors' density seems to have no significant influence on the global behavior (stiffness, failure mode, failure load) but it can influence the local behavior around the connectors. However, this result should be confirmed by further studies and an analytical model should be developed to establish the minimum number and maximum spacing of connectors assuring a full coupled behaviour.

Besides, the wood contribution to the hybrid beam depends strongly on the geometric configuration. In the case of full I steel profile, the wood contribution is low and can be neglected in the studied case where the steel stiffness is very high compared to that of wood. However, when one of the beam flanges is removed to obtain a tee cross-section, the wood beams increase by 20% the elastic bending

stiffness of the steel profile. In addition, it is observed that the wood contribution is higher in the nonlinear phase of behavior and near the ultimate state. Actually, the wood elements play the role of lateral supports for the steel profile against local instability and lateral torsional buckling increasing thus the ultimate resistance by more than 80 % for the studied configurations. It is remarked that the adopted test setup provided lateral restraint after hinge tilting, which may have an impact on the evaluation of the final capacity reduction factors.

The elastic behavior of the hybrid beams was modeled in a similar way as for the steel-concrete composite beams with full connections. The material characteristics are those obtained from tests. The comparison of the values obtained from the model and the tests shows that the discrepancies are about 10 %. Thus, the proposed approach can predict in acceptable manner the elastic behavior of hybrid beams. FE approaches that take into account the relative displacement between steel and wood for various conditions of connections may improve the accuracy of predictions.

At failure, the hybrid beams behavior was modeled by a multi-layer approach with innovative elastic-plastic combination. The timber beams was assumed to remain elastic with a strain limit to not be exceeded while it was assumed that the steel profile reach its full plastic capacity. The ultimate moment of the hybrid cross-section can be calculated analytically by solving a second-degree equation with parameters depending on the geometry and the material properties of the basic materials (wood and steel). The elastic instabilities are taken into account only for the steel profiles, by a reduction factor obtained from Eurocode 3 approach. In the frame of this conservative approach, this factor was calculated neglecting the stabilization effect of the wood beam on the steel profile regarding the lateral-torsional effect. However, the wood effect is considered as it allows the cross-section to reach its full plastic capacity. The comparison of the numerical and experimental results shows the relevance of the proposed approach. However, the evaluation of the reduction factor should be improved, especially in the case of tee sections.

This study confirms the advantages that can be obtained with the combination of steel and wood in hybrid structures in comparison with the use of steel or wood separately. The studied geometric configurations can be extended to various configurations including thin-walled cross-sections. In these cross-sections, as the instability is the main parameter to be observed, the contribution of wood can be maximized and the steel optimized. The present study is used as a basis to develop analytical and numerical models that can be used to predict the contribution of wood connected to steel profiles of various geometries and panel slenderness. This contribution needs to be calibrated considering various types of connections and geometries, regarding the local and lateral-torsional buckling of hybrid beams. A study is also in progress to evaluate the effect of wood on the fire resistance of hybrid beams. Actually, the wood contribution needs to be evaluated considering its insulation effect and lateral support against the local buckling of steel elements exposed to fire.

## References

- [1] Piazza M., Optimization process in the use of wood and wood-based materials in hybrid and composite structures, World Conference on Timber Engineering (WCTE 2016), Vienna, 2016, 10 pages.
- [2] Zhang X., Shahnewaz M., Tannert T., Seismic reliability analysis of a timber steel hybrid system, *Engineering Structures* 167 (2018) 629–638.
- [3] Koshihara M., Isoda H., Yusa S., The design and installation of a five-storey new timber building in Japan, international symposium on timber structure, Istanbul, Turkey, 11 pages, 2009.
- [4] Hassanieh A., Valipour H.R., Bradford M.A., Experimental and numerical study of steel-timber composite (STC) beams, *Journal of Constructional Steel Research* 122 (2016) 367–378.
- [5] Bradford M. A., Hassanieh A., Valipour H. R., Foster S. J., Sustainable steel-timber joints for framed structures, *Modern Building Materials, Structures and Techniques, MBMST 2016, Procedia Engineering* 172 (2017) 2-12.
- [6] Loss C., Davison B., Innovative composite steel-timber floors with prefabricated modular Components, *Engineering Structures* 132 (2017) 695–713.

- [7] Loss C., Piazza M., Zandonini R., Connections for steel–timber hybrid prefabricated buildings. Part I: Experimental tests, *Construction and Building Materials* 122 (2016) 781-795.
- [8] Bulleit W. M., Reinforcement of Wood materials: a review, *Wood and Fiber Science*, 16 (1984), 391-397.
- [9] Bulleit W. M., Sandberg B. L., Woods Greg J., Steel-reinforced glued laminated timber, *Journal of Structural Engineering*, vol.115 (1989), 433-444.
- [10] Borri A., Corradi M., Grazini A., FRP reinforcement of wood elements under bending loads, *Proceedings, Structural Faults and repair*, London, 14 pages, 2003.
- [11] Alam P., Ansell M.P., Smedley D., Mechanical repair of timber beams fractured in flexure using bonded in reinforcements, *Composites: Part B*, 40 (2009), 95–106.
- [12] Borri A., Corradi M., Strengthening of Timber Beams with high strength steel cords, *Composites Part B : Engineering*, vol 42 (2011), 1480-1491.
- [13] Borri A, Corradi M, Grazini A, A method for flexural reinforcement of old wood beams with CFRP materials, *Composite Part B: Engineering*, vol 36 (2005) 143-153.
- [14] Schober K., Harte A. M., Kliger R., Jockwer R., Xu Q., Chen J., FRP reinforcement of timber structures, *Construction and building materials*, 97 (2015),106-118.
- [15] Ghanbari-Ghazijahani T., Russo T., Valipour H.R., Lightweight timber I-beams reinforced by composite materials, *Composite Structures*, vol 233 (2020), 111579.
- [16] Jasienko J, Nowak TP, Solid timber beams strengthened with steel plates – Experimental studies, *Construction and building materials*, vol 63 (2014), 81-88.
- [17] Nowak TP, Jasienko J, Kotwica E, Krzosek S, Strength enhancement of timber beams using steel plates – Review and experimental tests, *Drewno*, vol 59 (2016), 75-90.
- [18] Alam P., Ansell M.P., The Effects of Varying Nailing Density upon the Flexural Properties of Fitch Beams, *Journal of Civil Engineering Research*, vol.2 (2012), 7-13.
- [19] Corradi M, Osofero AI, Borri A, Repair and Reinforcement of Historic Timber Structures with Stainless Steel - A Review, *Metals*, vol 9, (2019), 8-24.
- [20] Awaludina A., Rachmawatia K., Aryatia M., Danastria A. D., Development of cold formed steel – timber composite for roof structures: compression members, *Procedia Engineering* 125 (2015) 850 – 856.
- [21] Irawati I.S., Awaludina A., Sebastian N.P., The performance of cold-formed steel long-pan roof structures combined with laminated timber: cold-formed steel – laminated timber composite *Procedia Engineering* 171 (2017) 1242 – 1249.
- [22] Winter W., Tavoussi K., Riola Parada F., Bradley A., Timber-steel hybrid beams for multi-storey buildings: final report, *World Conference on Timber Engineering (WCTE 2016)*, Vienna, 2016, 10 pages.
- [23] Hu Q., Gao Y., Meng X., Diao Y., “Axial compression of steel-timber composite column consisting of H-shaped steel and glulam”, *Engineering Structures*, vol. 216, 12 pages, 2020.
- [24] Alam P., “The reinforcement of timber for Structural Applications and Repair”, PhD thesis, University of Bath, 2004.
- [25] NF B 52-001-2, “Regulations governing the use of timber in structure – Visual classification for the use of French softwood and hardwood species in structures – Part 2: Alternative method for massif wood for manufacturing glued laminated timber BLC and glued solid timber BMR”, 2011 (in French).
- [26] NF 13183-1, “Moisture content of a piece of sawn timber – Part 1: Determination by oven dry method”, 2002.
- [27] EN 408, “Timber Structures – Structural timber and glued laminated timber – Determination of some physical and mechanical properties”, 2009.
- [28] Eurocode 4, Design of composite steel and concrete structures, Part 1-1: General rules and rules for buildings. European Committee for Standardization (CEN), London (UK), (2004).
- [29] EN 1993-1-1, “Eurocode 3: Design of steel structures – Part 1.1: General rules for buildings”, 2005.
- [30] LTBeam, software developed by the CTICM for the calculation of lateral buckling critical bending moment, ECSC Project No 7210-PR183 : "Lateral torsional buckling of steel and composite beams" - 1999-2002. <https://www.cticm.com/content/ltbeam-logiciel-calcul-moment-critique-deversement>.

- [31] Deskovic N, Triantafillou TC, Meier U. Innovative Design of FRP Combined with Concrete: Short-Term Behavior, *J Struct Eng*, 121 (1995).
- [32] Correia JR, Branco FA, Ferreira JG. Flexural behavior of GFRP-concrete hybrid beams with interconnection slip. *Compos Structures*, 77 (2007):66–78.
- [33] Koaik A., Bel S., Jurkiewicz B., Experimental and Analytical Analysis of Concrete-GFRP Hybrid Beams under flexure, *Composites Structures*, 180 (2017), 192-210.